Influence of failed blade-pitch-control system to FOWT by aero-elastic-control-floater-mooring coupled dynamic analysis

Yoon Hyeok Bae[*] and Moo-Hyun Kim

Department of Civil Engineering, Texas A&M University, College Station, TX, USA

Abstract. More FOWTs (floating offshore wind turbines) will be installed as relevant regulations and technological hurdles are removed in the coming years. In the present study, a numerical prediction tool has been developed for the fully coupled dynamic analysis of FOWTs in time domain including aero-loading, tower elasticity, blade-rotor dynamics and control, mooring dynamics, and platform motions so that the influence of rotor-control dynamics on the hull-mooring performance and vice versa can be assessed. The developed coupled analysis program is applied to Hywind spar design with 5 MW turbine. In case of spar-type floaters, the control strategy significantly influences the hull and mooring dynamics. If one of the control systems fails, the entire dynamic responses of FOWT can be significantly different. Therefore, it is important to maintain various control systems in a good operational condition. In this regard, the effects of failed blade pitch control system on FOWT performance including structural and dynamic responses of blades, tower, and floater are systematically investigated. Through this study, it is seen that the failure of one of the blade pitch control system can induce significant dynamic loadings on the other blades and the entire FOWT system. The developed technology and numerical tool are readily applicable to any types of floating wind farms in any combinations of irregular waves, dynamic winds, and steady currents.

Keywords: floating wind turbine; spar type; simulation; aero-elastic-control-floater-mooring coupled dynamics; blade-pitch-control failure; blade/tower/platform responses; structural health monitoring

1. Introduction

Wind is the fastest-growing clean and renewable energy source. Until recently, most of the offshore wind-farm development has been limited to shallow-water areas. However, there exist negative features of shallow-water development, which include lack of available space, noise restriction, shade/visual pollution, community opposition, and harsher regulatory problems.

In this regard, several countries started to plan floating offshore wind farms in deeper waters. Although they are considered to be more difficult to design and operate, wind farms in deeper waters are in general less sensitive to space availability, noise restriction, visual pollution and regulatory problems. They are also exposed to much stronger and steadier wind field to be more effective. Furthermore, in designing those floating wind farms, the existing technology and experience of offshore oil & gas industry is directly applicable. If the relevant technology and infrastructure are fully developed, offshore floating wind turbines are expected to produce huge

---
∗Corresponding author, Postdoctoral Research Associate, E-mail: yoonhyeok.bae@tamu.edu

amount of clean electricity at a competitive price compared to other energy sources (Henderson *et al*. 2002, Henderson *et al*. 2004, Musial *et al*. 2004, Tong 1998).

For floating wind turbines, their natural frequencies of 6-DOF motions are typically much lower than those rotor-induced or tower-flexibility-induced excitations, so the possibility of dynamic resonance is low (Jonkman and Sclavounos 2006, Withee 2004). One exception is the TLP-type OWT (Bae *et al*. 2010, 2011, Jagdale and Ma 2010) which is much stiffer in the vertical-plane modes compared to other floating wind turbines, and thus the effects of such high-frequency excitations from the tower and blades need to be checked (Bae and Kim 2013a). For spar or semi-submersible floaters (Roddier *et al*. 2009), the low-frequency excitations related to blade pitch-angle control may cause large-amplitude slowly-varying floater motions (Nielsen *et al*. 2006). Therefore, the accurate estimation of the coupling effects between the floater dynamics and control-induced actuation forces is very important in the optimal design of such floating OWTs.

In this regard, an aero-elastic-control-floater-mooring coupled dynamic analysis computer program is developed by combining several modules. For the dynamic analysis and control of wind turbine system, the primary design code of wind turbines, FAST, developed by National Renewable Energy Laboratory (NREL) is employed (Jonkman 2003, 2007, 2008, Jonkman and Buhl Jr. 2004). The FAST is implemented into the floater-mooring coupled dynamic analysis program, CHARM3D, which has been developed by authors' group during the past decade (Kim *et al*. 2001, Tahar and Kim 2003, Yang and Kim 2010, 2011, Kang and Kim 2012). The two programs are modified/combined so that the entire system can be solved in time domain by a global combined matrix including all the relevant coupling forces and degrees of freedom. As a result, the dynamic time histories of the FOWT system including full couplings among tower, blade, drive-train, floater, and mooring can be obtained simultaneously by a single run.

In this paper, the developed computer program is applied to the analysis of a 5 MW spar-type FOWT designed for 320 m water depth to study the effects of failed blade-control strategies on the global performance and local structural loadings. The effects of the rotor imbalance induced by the failed blade pitch control are presented in time domain. Similar research about the global/local performance of TLP-type FOWT with partially broken blade was conducted in Bae and Kim (2013b). It showed that the unbalanced-loadings from the blades may induce additional excitations and responses in the tower and blade dynamics.

The FOWT is unmanned offshore platforms and a remote health monitoring strategy needs to be developed for structural safety and effective maintenance. This kind of simulation tool with systematic failure scenarios may help to develop such a system. The simulation tool can also be used for the forensic investigations to detect the cause of failure incidents.

2. Numerical analysis of 5 MW floating wind turbine in time domain

The time-domain simulation tool for rotor-floater-control-mooring fully-coupled dynamic analysis is applied in this study to the 5 MW Hywind spar-type FOWT system. In order to couple the wind-turbine module and the mooring/floater dynamics module, two different computer programs, FAST and CHARM3D, are combined and modified to better understand their full coupling effects by solving them simultaneously in a combined matrix system. The hydrodynamic coefficients including added mass, radiation damping, wave-frequency forces and second-order mean drift forces of floaters are obtained by the 3D diffraction/radiation preprocessor WAMIT in

frequency domain (Lee and Newman 1991) and the information is transferred to the time-domain analysis tool, CHARM3D. The mooring dynamics coupled with hull motions are solved at each time step by a generalized-coordinate-based finite element (FE) program using high-order elements, the details of which are given in Kim *et al.* (2001).

$$[M + M^a(\infty)]\ddot{\xi} + K\xi = F_I(t) + F_c(t,\dot{\xi}) + F_n(t,\dot{\xi}) + F_m(t) \tag{1}$$

where $M^a(\infty)$ denotes added mass at infinite frequency, M the system mass matrix, K the system hydrostatic stiffness matrix, $F_I(t)$ the first and second order wave exciting forces including both Froud-Krylov and diffraction components, and $F_n(t,\dot{\xi})$ the nonlinear drag force from Morison's equation at the instantaneous wet position. The drag force is proportional to the fluid-body relative velocity squared, so it contributes to both viscous damping force and viscous exciting force. $F_m(t)$ the mooring force and $F_c(t,\dot{\xi})$ the radiation damping force as follows

$$F_c(t,\dot{\xi}) = -\int_{-\infty}^{t} R(t-\tau)\dot{\xi}(\tau)d\tau \tag{2}$$

$\xi, \dot{\xi}$, and $\ddot{\xi}$ represent the 6-DOFs displacements, velocities, and accelerations of the floating body. $R(t)$ is the retardation function.

The complete nonlinear aero elastic equations of motion for the wind turbine model is

$$M(\underline{q},\underline{u},t)\ddot{\underline{q}} + f(\underline{q},\dot{\underline{q}},\underline{u},\underline{u}_d,t) = \underline{0} \tag{3}$$

where M is the mass matrix, f is the forcing function, $\underline{u}$ and $\underline{u}_d$ are the set of wind turbine control inputs and wind inputs, respectively. $\underline{q}$, $\dot{\underline{q}}$, and $\ddot{\underline{q}}$ are the vectors of wind turbine motions, velocities, and accelerations, and t is time.
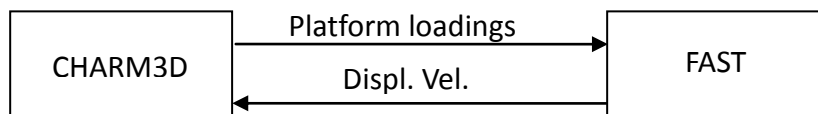

Fig. 1 Basic concept of FAST-CHARM3D coupling

The wind turbine dynamics including 6-DOF platform dynamics are computed by FAST. CHARM3D calculates all of the external forces acting on the platform, and feeds the external forces to FAST at each time step. The transferred external forces include first-order and second order wave forces, radiation damping force, nonlinear viscous drag force from Morison members, and mooring-induced restoring force. The mooring restoring force can be estimated by the top tension of each mooring line and its directional cosine. Then FAST fills out the forcing function in Eq. (3) using those transferred forces, and solves displacements, velocities, and accelerations of all

degrees of freedom including elastic responses. Those obtained platform kinematic data are then fed into CHARM3D side in order to update external forces. The procedure is repeated for the next time step. For the present simulation, the time step of CHARM3D is 0.05s and the internal time step for FAST-side is 0.0125s, which means that at every time interval of CHARM3D, the FAST internally calculates 4 steps, and return the resultant data to CHARM3D. Its accuracy was checked by a more conservative approach by using 0.0125s for both programs. The basic concept of rotor-floater coupling is schematically shown in Fig. 1.

The control system of the 5 MW wind turbine consists of variable-speed and variable-blade-pitch-to-feather controller. The two control strategies work together to produce quality power and keep the entire system in good condition. Typical control strategies of land-based turbine can directly be applicable to TLP-type offshore wind turbines without any significant modification due to their limited rotational motions (roll, pitch and yaw). However in case of spar-type offshore wind turbines, it is necessary to change the control strategy to ensure smooth operation and higher-quality power generation. In this study, the modified control strategy which is optimized for a spar-type FOWT was used. For the accurate estimation of the global performance of the FOWT system with the respective control strategies, a reliable rotor-floater-mooring coupled dynamic analysis tool is essential.

Table 1 Specifications of 5 MW turbine

Item	Unit	Value
Tower height	m	90.0
Rotor diameter	m	126.0
Tower diameter (top)	m	3.87
Tower diameter (bottom)	m	6.5
Elevation to Tower Base above SWL	m	10.0
Elevation to Tower Top above SWL	m	87.6
Overall Tower mass	kg	249,718
Total wind turbine weight (except for platform)	kg	599,718
CM Location of Tower above SWL Along Tower Centerline	m	43.4
Tower Structural Damping Ratio (All modes)	%	1.0

Table 2 Specifications of Hywind spar platform

Item	Unit	Value
Depth to Platform Base below SWL (Total Draft)	m	120.0
Elevation to Platform Top Above SWL	m	10.0
Depth to Top of Taper Below SWL	m	4.0
Depth to Bottom of Taper Below SWL	m	12.0
Platform Diameter Above Taper	m	6.5
Platform Diameter Below Taper	m	9.4
Platform Mass, including Ballast	kg	7,466,330
CM Location Below SWL Along Platform Centerline	m	89.9155
Platform Roll Inertia about CM	kg·m^2	4,229,230,000
Paltform Pitch Inertia about CM	kg·m^2	4,229,230,000
Platform Yaw Inertia about Platform Centerline	kg·m^2	164,230,000

The adopted model of 5 MW turbine is the 'National Renewable Energy Laboratory (NREL) offshore 5 MW baseline wind turbine' which has been adopted as the reference model for the integrated European UpWind research program. Hywind floating platform in this paper is the 'OC3-Hywind' spar-buoy-type platform which is slightly different from the turbine used by Statoil-Norway. The detailed specifications of the 5MW turbine and Hywind spar are tabulated in Tables 1 and 2.

The Hywind spar is moored by a system of three catenary lines. To increase the yaw stiffness of the platform, the lines are attached to the hull via delta connection. This delta-connection effect is included in the time-domain simulation by adding yaw spring stiffness. The specifications of mooring system are tabulated in Table 3.

Table 3 Specifications of Hywind spar mooring system

Item	Unit	Value
Number of Mooring Lines	ea	3
Angle Between Adjacent Lines	deg	120
Depth to Anchors Below SWL (Water Depth)	m	320
Depth to Fairleads Below SWL	m	70.0
Radius to Anchors from Platform Centerline	m	853.87
Radius to Fairleads from Platform Centerline	m	5.2
Unstretched Mooring Line Length	m	902.2
Mooring Line Diameter	m	0.09
Equivalent Mooring Line Mass Density	kg/m	77.7066
Equivalent Mooring Line Weight in Water	N/m	698.094
Equivalent Mooring Line Extensional Stiffness	N	384,243,000
Additional Yaw Spring Stiffness	Nm/rad	98,340,000

Each mooring line is modeled by 20 high-order finite elements, and its unstretched length is 902.2 m. Illustrations of mooring-line arrangement are shown in Fig. 2.
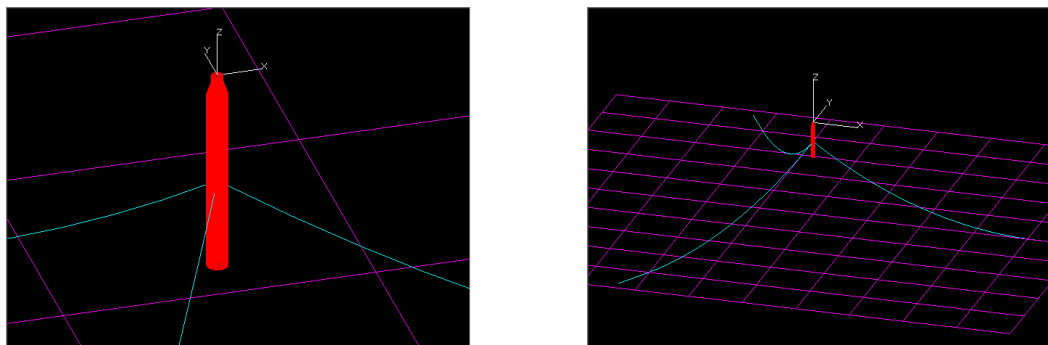

Fig. 2 Mooring-line arrangement

The natural frequencies of the Hywind spar platform are tabulated in Table 4.

Table 4 Natural frequencies of platform motions

Mode	Surge	Sway	Heave	Roll	Pitch	Yaw
Frequency (rad/s)	0.05	0.05	0.20	0.22	0.22	0.71

3. Failure of blade pitch control system

For the NREL 5MW turbine, two control systems are designed to work. A generator-torque controller and a blade-pitch controller are working in the below-rated and above-rated wind-speed range, respectively. The generator-torque controller is designed to maximize power capture and the blade-pitch controller is designed to regulate generator speed by gain-scheduled proportional-integral (PI) control. In this study, one of the blade pitch actuator is assumed to be locked and does not work while the others work properly as depicted in Fig. 3. For this simulation, the blade-pitch controller is assumed to work individually.
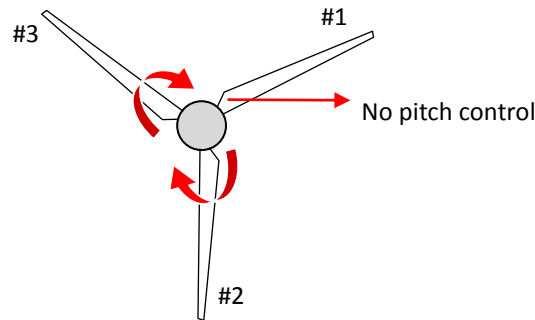

Fig. 3 Failed blade pitch control

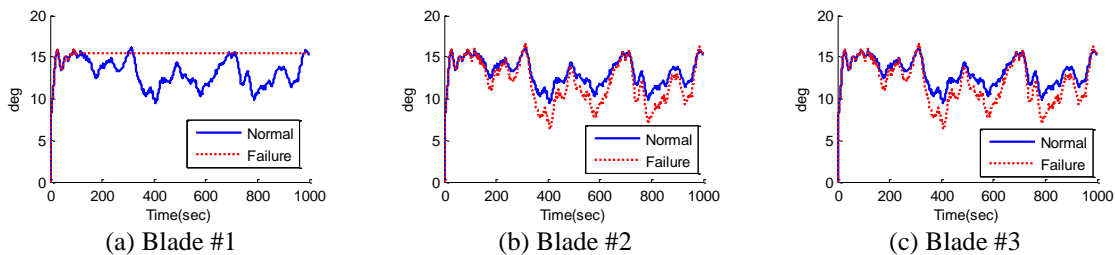| (a) Blade #1	(b) Blade #2	(c) Blade #3

Fig. 4 Blade pitch angle time histories with failure after 100 seconds

In time-domain simulation, the total simulation time is set to 1,000 seconds, and the mal-function of the blade pitch control occurs at 100 seconds. The failed blade pitch angle is locked at 100 seconds and fixed at 15.4 degrees for the remaining time. The time histories of blade pitch angle are shown in Fig. 4.

   In Fig. 4(a), the blade pitch angle in dotted line is fixed at 15.4 degrees which is the final pitch angle at 100 seconds. Since the pitch angle is fixed at relatively higher angle, the thrust force from the wind is decreased accordingly. To maintain the rotor speed and to compensate the loss of thrust force, the other two blades start to lower the pitch angles as can be seen in Figs. 4(b) and 4(c). For example, the minimum pitch angle of 9.5 degrees in normal condition goes down to 6.4 degrees. As a result, the total thrust force of the rotor remains at a normal level and the decrease of the generated electricity can be minimized.

   The changes in the blade pitch angles also affect the blade root shear forces. In the case of blade #1, the overall shear force after failure decreased due to the loss of the aerodynamic loading, while the other blades show the increased mean/max shear forces as can be seen in Fig. 5. The statistics in Table 5 indicate that the mean shear force of blade 1# is decreased by 33.3%. On the contrary, the mean shear forces of blade #2 and #3 are increased by 12.3% and 22.5%, respectively. The standard deviations of the shear forces are also increased by 14.0~31.4%, which means that the blade roots in failure condition are more prone to the fatigue damage.
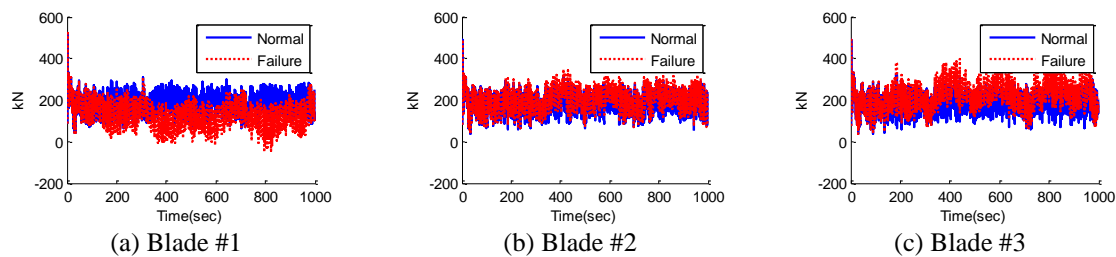

| (a) Blade #1 | (b) Blade #2 | (c) Blade #3 |

Fig. 5 Blade flapwise shear force with failure after 100 seconds

Table 5 Statistics of blade flapwise shear force with failure after 100 seconds

		Max.	**Min**	**Mean**	**SD**
Blade #1	Normal	3.082E+02	5.948E+01	1.828E+02	4.250E+01
(kN)	Failure	3.104E+02	-5.092E+01	1.219E+02	5.160E+01
Blade #2	Normal	3.083E+02	5.253E+01	1.826E+02	4.243E+01
(kN)	Failure	3.468E+02	6.472E+01	2.051E+02	4.837E+01
Blade #3	Normal	3.185E+02	4.328E+01	1.824E+02	4.315E+01
(kN)	Failure	3.946E+02	4.717E+01	2.236E+02	5.668E+01

   In the case of maximum and mean shear forces between blades #2 and #3, the latter has greater responses. This results are strongly related to the order of blade arrangement and the platform yaw motion induced by asymmetric loadings on the blades. In detail, the blade root shear force is determined by both blade inertial loading and aerodynamic loading. The blade inertial loadings may differ from each blade depending on the instantaneous blade position and the platform yaw acceleration. In this study, the platform yaw period is strongly correlated with the 1P frequency excited by the mal-functioned blade #1. 1P represents the once-per-revolution frequency of the rotor (1.27 rad/s) and it can be obtained from the rated rpm (12.1 rpm here). Since rotor frequency and platform yaw frequency coincide, each blade root shear force shows repeated pattern and one

can be statistically higher than the others. This phenomenon can be confirmed by yawing turbine model and steady wind test. In Fig. 6, the azimuth angles of the blades where their root shear force is maximum in the steady state condition are depicted. In the steady state condition, each blade always has its maximum shear force near the designated point and each maximum shear force is determined by the instantaneous position, platform yaw acceleration, and aerodynamic loading at that time. If the platform yaw motion is restricted or the turbine is land-based, this phenomenon cannot be observed and the maximum or mean level of the blades #2 and #3 will be similar.
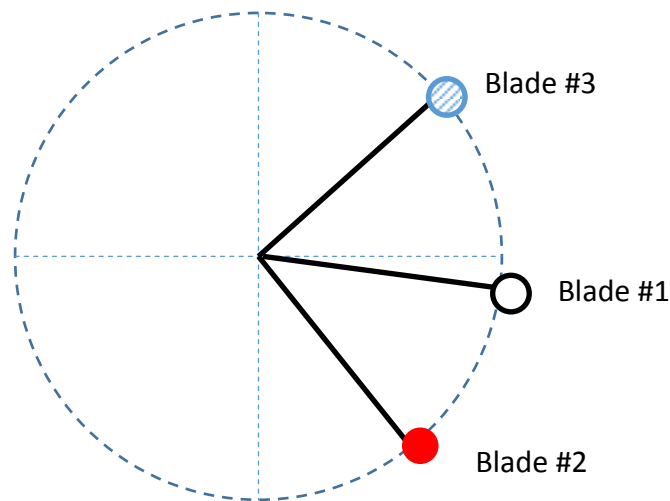

Fig. 6 Azimuth point of maximum blade root shear force

Furthermore, the aerodynamic loading on the blades with wind shear along the vertical direction also contribute to the trend of the blade root shear forces. In summary, the differences of maximum and mean shear forces between blade #2 and #3 are made by the combination of 1P rotation of rotor, 1P-yaw-motion induced inertial loading, and aerodynamic loading on each blade.

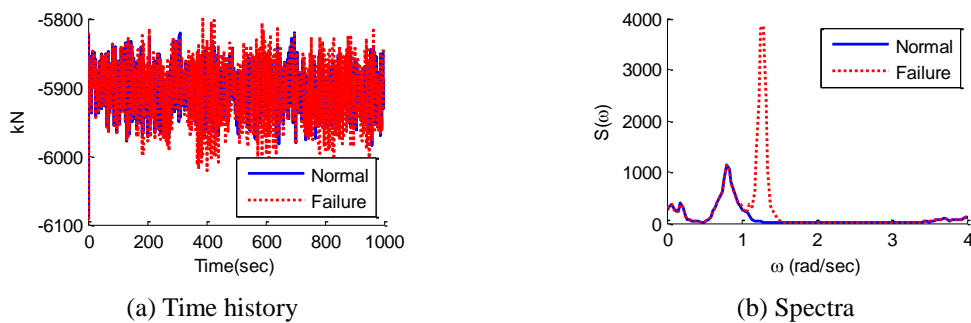(a) Time history   (b) Spectra

Fig. 7 Tower base axial force

The statistics in Table 6 shows the dramatic changes of torsional moment of tower base

between the normal and failure cases. The maximum torsional moment after failure is increased by 96.9% and the maximum of the opposite-direction torsional moment is increased up to 138.4%. So, the structural failure of the tower base may occur if the safety factor is not enough to cover these load variations.

Table 6 Statistics of tower base loads

		Max.	**Min**	**Mean**	**SD**
Axial	Normal	-5.822E+03	-5.985E+03	-5.907E+03	2.439E+01
(kN)	Failure	-5.801E+03	-6.021E+03	-5.908E+03	3.413E+01
Torsional	Normal	4.260E+03	-4.240E+03	-3.340E+02	1.087E+03
(kN·m)	Failure	8.389E+03	-1.011E+04	-3.171E+02	2.871E+03

Though the drag force of blade #1 is decreased, the overall rotor thrust force shows similar level with the normal case because the deficit of aerodynamic loading from blade #1 is compensated by the other blades. In Fig. 9, it is seen that the rotor thrust force after failure does not make big difference except for the very small additional excitation near the 1P frequency.
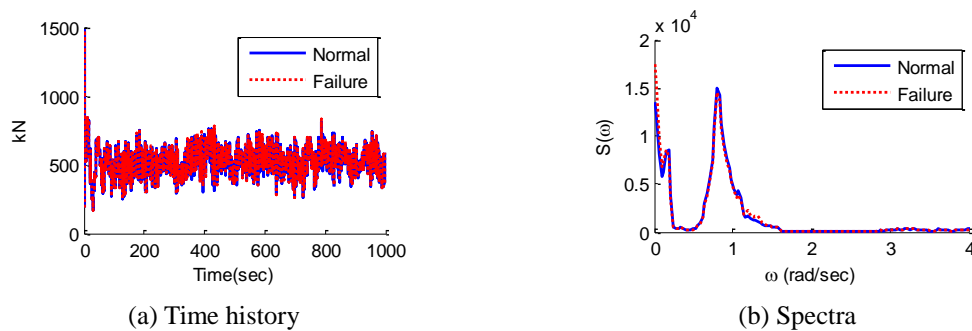

(a) Time history	(b) Spectra

Fig. 9 Rotor thrust force

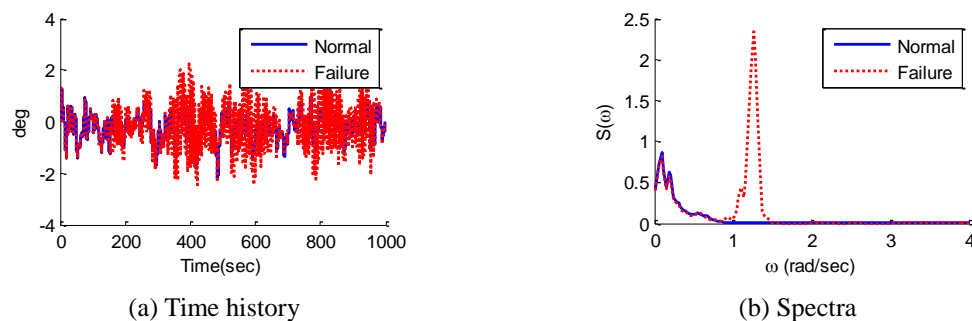| (a) Time history	(b) Spectra

Fig. 10 Platform yaw motion

The blade-pitch-control failure also affects the dynamic response of the floating platform. Fig. 10 shows the platform yaw motion and its spectrum. Compared to the normal case, the peak near the 1P frequency is very clear and the yaw motion becomes larger than that of the normal case. The maximum platform yaw angle is increased from 1.05 degrees to 2.26 degrees and the standard deviation after failure is higher than that of normal case by 58.9%.

So far, the simulation was carried out when the blade pitch angle is locked after 100 seconds. In that simulation, the final pitch angle was 15.4 degrees which reduced the aerodynamic loading on that blade considerably compared to the other blades. The simulation can also be done with different locking time and associated final pitch angle. For example, if the blade pitch actuator is locked at 400 seconds, then the final blade pitch angle is 9.98 degrees which is lower than the previous case. In this case, the aerodynamic loading on the blade #1 increases and the corresponding blade pitch angles of blade #2 and #3 increase as can be seen in Fig. 11. The transient effects at the moment of failure do not seem to be significant.
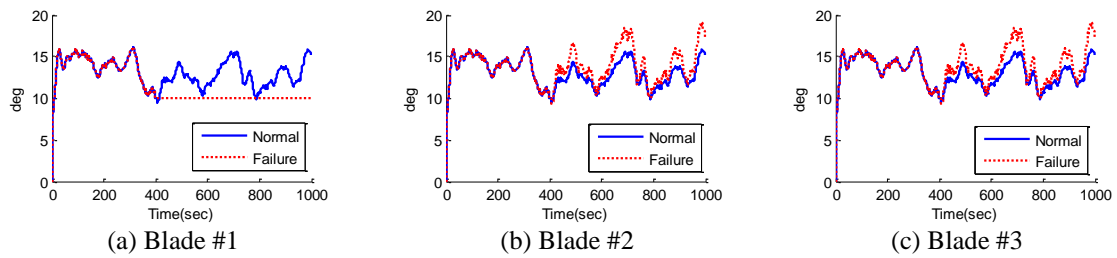

(a) Blade #1   (b) Blade #2   (c) Blade #3

Fig. 11 Blade-pitch-angle time histories with failure after 400 seconds

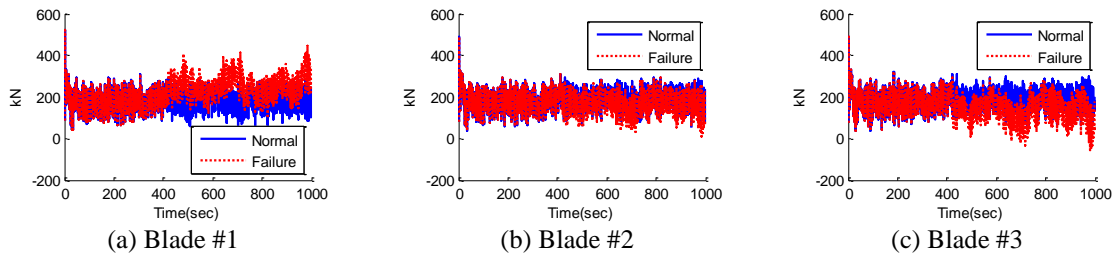(a) Blade #1   (b) Blade #2   (c) Blade #3

Fig. 12 Blade flapwise shear force with failure after 400 seconds

The resultant blade flapwise shear forces are depicted in Fig. 12. The increased aero loading of blade #1 results in the higher shear force, while the shear forces from the other blades show lower mean values compared to the normal case. For instance, the mean shear force of blade #1 is increased by 24.9%, while the mean shear forces of the other blades are decreased by 8~16.3% as can be seen in Table 7. In this example, the mean and minimum shear forces between blades #2 and #3 after 400 seconds also show noticeable difference and it can be explained in a similar way as pointed out before. Depending on the phase differences between platform yaw motion and the rotor rotation, the maximum or minimum shear forces may vary.

Table 7 Statistics of blade flapwise shear force with failure after 400 seconds

		Max.	Min	Mean	SD
Blade #1	Normal	3.082E+02	5.948E+01	1.828E+02	4.250E+01
(kN)	Failure	4.474E+02	6.200E+01	2.283E+02	6.038E+01
Blade #2	Normal	3.083E+02	5.253E+01	1.826E+02	4.243E+01
(kN)	Failure	3.093E+02	6.952E+00	1.680E+02	4.731E+01
Blade #3	Normal	3.185E+02	4.328E+01	1.824E+02	4.315E+01
(kN)	Failure	3.185E+02	-5.337E+01	1.526E+02	5.442E+01

Other than the final blade pitch angle of failed blade and associated blade structural responses, the tower base loadings and the platform yaw responses show similar trend as already presented in Figs. 7-10. Since aerodynamic loadings are unbalanced, the same 1P response is detected in various responses of FOWT such as tower base torsional moment and platform yaw motion. The unbalanced loadings on the blades significantly reduce the fatigue life of the structural members, so it is important to check the structural integrity with various turbine failure scenarios.

4. Conclusions

The dynamic responses of a Hywind spar-type floating wind turbine with partially failed blade pitch control are investigated. Through this study, it is seen that the effect of partial blade-pitch-control failure can be significant regardless of the final pitch angle. Specifically, the platform yaw responses and the tower-base torsional moments are the most serious changes. The tower-base loads and blade-root shear forces can also be increased with the failed condition. Due to the rotational imbalance with the failure, the 1P excitations and responses are more pronounced in the tower and blade dynamics. One of the interesting points in this study is that the blade root shear forces of the two remaining blades show different mean and maximum loadings, which is related to the platform-yaw-induced inertial loading on the blade. The repetitive behavior of the inertial loading is strongly related to the overlap between the 1P platform yaw and blade rotation.

To avoid the local fatigue failure or the collapse of entire system due to the unbalanced loadings from the blades, the structural integrity with various failure scenarios, especially for the yaw-related responses, should be carefully checked. The present approach for FOWT can directly be applied to the development of remote structural health monitoring system in detecting the failure of blade pitch control or the partial loss of system mass/stiffness.

Acknowledgments

References

Bae, Y.H., Kim, M.H. and Shin, Y.S. (2010), "Rotor-floater-mooring coupled dynamic analysis of mini TLP-type offshore floating wind turbines", *Proceedings of the ASME 29th International Conference on Ocean, Offshore and Arctic Engineering*, Shanghai, China.

Bae, Y.H. and Kim, M.H. (2013a), "Rotor-floater-tether coupled dynamics including second-order sum–frequency wave loads for a mono-column-TLP-type FOWT (floating offshore wind turbine)", *Ocean Eng*., **61**, 109-122.

Bae, Y.H. and Kim, M.H. (2013b), "Coupled dynamic analysis of FOWT (Floating Offshore Wind Turbine) with partially broken blade", *Proceedings of the 23rd International Offshore and Polar Engineering Conference*, Anchorage, AK.

Bae,Y.H. and Kim, M.H. (2011), "Rotor-floater-mooring coupled dynamic analysis of mono-column-TLP-type FOWT (Floating Offshore Wind Turbine)", *Ocean Syst. Eng*., **1**(1), 93-109

Henderson, A., Leutz, R. and Fujii, T. (2002), "Potential for floating offshore wind energy in Japanese waters", *Proceedings of the 12th International Offshore and Polar Engineering Conference*, Kitakyushu, Japan.

Henderson, A.R., Zaaijer, M., Bulder, B., Pierik, J., Huijsmans, R., van Hees, M., Snijders, E., Wijnants, G.H. and Wolf, M.J. (2004), "Floating windfarms for shallow offshore sites", *Proceedings of the 22nd International Offshore and Polar Engineering Conference*, Toulon, France.

Jagdale, S. and Ma, Q. (2010), "Practical simulation on motions of a TLP-type support structure for offshore wind turbines", *Proceedings of the 20th International Offshore and Polar Engineering Conference*, Beijing, China.

Jonkman, J.M. (2003), *Modeling of the UAE Wind Turbine for Refinement of FAST_AD*, National Renewable Energy Laboratory, Golden, CO.

Jonkman, J.M. and Buhl Jr, M.L. (2004), *FAST user's guide*, National Renewable Energy Laboratory, Golden, CO.

Jonkman, J.M. and Sclavounos, P.D. (2006), *Development of fully coupled aeroelastic and hydrodynamic models for offshore wind turbines*, Paper presented at the 44th AIAA Aerospace Sciences Meeting and Exhibit, Reno, NV.

Jonkman, J.M. (2007), *Dynamics modeling and loads analysis of an offshore floating wind turbine*, National Renewable Energy Laboratory, Golden, CO.

Jonkman, J.M. (2008), "Influence of control on the pitch damping of a floating wind turbine", *Proceedings of the ASME Wind Energy Symposium*, Reno NV.

Kang, H.Y. and Kim, M.H. (2012), "Hydrodynamic interactions and coupled dynamics between a container ship and multiple mobile harbors", *Ocean Syst. Eng*., **2**(3), 217-228

Kim, M.H., Tahar, A. and Kim, Y.B. (2001), "Variability of TLP motion analysis against various design methodologies/parameters", *Proceedings of the 11th International Offshore and Polar Engineering*, Stavanger, Norway.

Lee, C.H. and Newman, J.N. (1991), *First-and second-order wave effects on a submerged spheroid*.

Musial, W.D., Butterfield, S. And Boone, A. (2004), "Feasibility of floating platform systems for wind turbines", *Proceedings of the 42nd AIAA Aerospace Sciences Meeting and Exhibit*, Reno, NV.

Nielsen, F.G., Hanson, T.D. and Skaare, B. (2006), "Integrated dynamic analysis of floating offshore wind turbines", *Proceedings of the ASME 25th International Conference on Offshore Mechanics and Arctic Engineering*, Hamburg, Germany.

Roddier, D., Cermelli, C. and Weinstein, A. (2009), "Windfloat: a floating foundation for offshore wind turbines part i: design basis and qualification process", *Proceedings of the ASME 28th International Conference on Ocean*, Offshore and Arctic Engineering, Honolulu, HI.

Tahar, A. and Kim, M.H. (2003), "Hull/mooring/riser coupled dynamic analysis and sensitivity study of a tanker-based FPSO", *Appl. Ocean Res*., **25**(6), 367-382.

Tong, K. (1998), "Technical and economic aspects of a floating offshore wind farm", *J. Wind Eng. Ind. Aerod*., **74**, 399-410.

Withee, J.E. (2004), *Fully coupled dynamic analysis of a floating wind turbine system*, Doctoral thesis, Massachusetts Institute of Technology.

Yang, C.K. and Kim, M. (2010), "Transient effects of tendon disconnection of a TLP by hull–tendon–riser coupled dynamic analysis", *Ocean Eng*., **37**(8), 667-677.

Yang, C.K. and Kim, M.H. (2011), "The structural safety assessment of a tie-down system on a tension leg platform during hurricane events", *Ocean Syst. Eng*., **1**(4), 263-283.